Physicochemically Tunable Polyfunctionalized RNA Square Architecture with Fluorogenic and Ribozymatic Properties

Daniel L. Jasinski,[†] Emil F. Khisamutdinov,[†] Yuri L. Lyubchenko,[‡] and Peixuan Guo[†,*]

[†]Nanobiotechnology Center, Markey Cancer Center, and Department of Pharmaceutical Sciences, College of Pharmacy, University of Kentucky, Lexington, Kentucky 40536, United States and [‡]Department of Pharmaceutical Sciences, University of Nebraska Medical Center, Omaha, Nebraska 68198, United States

ABSTRACT Recent advances in RNA nanotechnology allow the rational design of various nanoarchitectures. Previous methods utilized conserved angles from natural RNA motifs to form geometries with specific sizes. However, the feasibility of producing RNA architecture with variable sizes using native motifs featuring fixed sizes and angles is limited. It would be advantageous to display RNA nanoparticles of diverse shape and size derived from a given primary sequence. Here, we report an approach to construct RNA nanoparticles with tunable size and stability. Multifunctional RNA squares with a 90° angle were constructed by tuning the 60° angle of the three-way junction (3WJ) motif from the packaging RNA (pRNA) of the bacteriophage phi29 DNA packaging motor. The physicochemical properties and size of the RNA square were also easily tuned by modulating the "core" strand and adjusting the length of the sides of the square *via* predictable design. Squares of 5, 10, and 20 nm were constructed, each showing diverse thermodynamic and chemical stabilities. Four "arms" extending from the corners of the square were used to incorporate siRNA, ribozyme, and fluorogenic RNA motifs. Unique intramolecular contact using the pre-existing intricacy of the 3WJ avoids relatively weaker intermolecular interactions *via* kissing loops or sticky ends. Utilizing the 3WJ motif, we have employed a modular design technique to construct variable-size RNA squares with controllable properties and functionalities for diverse and versatile applications with engineering, pharmaceutical, and medical potential. This technique for simple design to finely tune physicochemical properties adds a new angle to RNA nanotechnology.

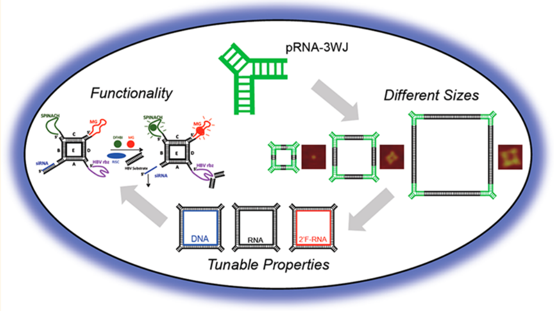

KEYWORDS: pRNA-3WJ motif · RNA nanostructure · nanobiotechnology · RNA nanotechnology · biomimetics

DNA, RNA, and proteins produce a variety of highly ordered nanoscale structures to perform diverse functions.[1−5] The intricacies of these natural biomaterials have inspired their applications as building blocks to fabricate sophisticated nanodevices.[6−17] In nanotechnology, RNA can be manipulated to assemble nanostructures with simple approaches as in DNA nanotechnology, while displaying versatility in structure and function similar to proteins. Thus, RNA has the advantage of two worlds, which garners tremendous interest in the directed design of a variety of RNA nanoarchitectures. Natural RNA molecules form a wide variety of complex structures by hierarchical folding that generates different motifs or modular units.[18,19] These modular units can be "manually" extracted and used to fabricate artificial self-assembling RNA complexes of diverse 1D, 2D, and 3D nanoarchitectures with novel and unique functional features.[2,16,20,21] Many RNA motifs exhibit phenomenal flexibility,[22−24] and the angles needed to form many nanoassemblies are encoded in the primary sequence of the structural motifs. The structure of a complex RNA architecture can be engineered by programming the information of a 3D structural motif into the nanoparticle's primary sequences. However, the flexibility of RNA motifs has seldom been used to construct diverse shaped nanoparticles utilizing the same core structure.

Previous work in this lab has detailed the construction of RNA nanoparticles utilizing the packaging RNA (pRNA) from the

* Address correspondence to peixuan.guo@uky.edu.

Received for review April 18, 2014 and accepted June 27, 2014.

10.1021/nn502160s

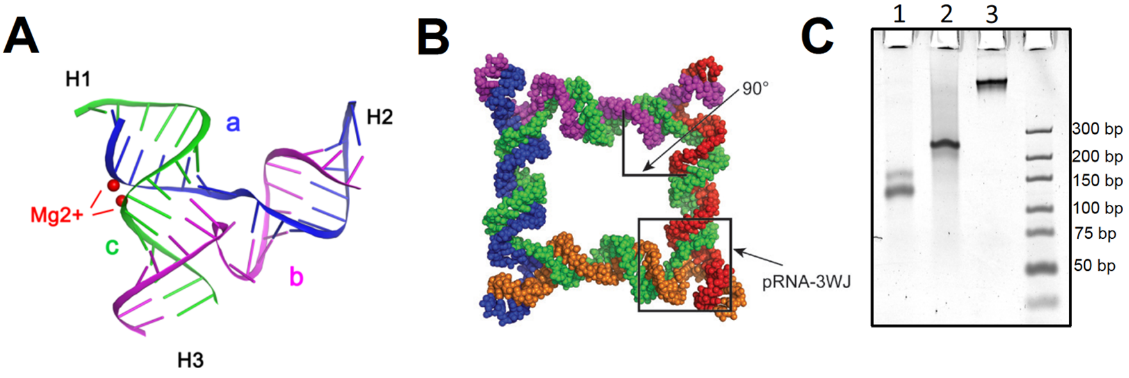

Figure 1. Design and assembly of the RNA squares. (A) Crystal structure of pRNA-3WJ showing the three-component strands of the pRNA-3WJ, a_{3WJ} (blue), b_{3WJ} (purple), and c_{3WJ} (green). (B) Three-dimensional structure of a square-shaped nanoparticle modeled on Swiss PDB Viewer, based on pRNA-3WJ. (C) Native PAGE assembly gel with ethidium bromide total RNA staining showing the assembly of each square structure: Lane 1 is 5 nm square, lane 2 is 10 nm square, lane 3 is 20 nm square.

bacteriophage phi29 DNA packaging motor. Dimers, trimers, tetramers, and hexamers have been constructed utilizing hand-to-hand and foot-to-foot interactions as well as arm extension technologies that implement kissing-loop, sticky-end, and complementary interactions.[1,20,25−30] Additionally, the three-way junction (3WJ) and X-way motifs from the phi29 motor pRNA themselves have proven successful as therapeutic delivery systems.[2,21,31] Other RNA nanoparticle-based delivery systems have shown potential as therapeutic carriers.[15,32−39]

Size and shape play an important role in the delivery efficacy, biodistribution, and circulation time of nanoparticles.[40] Control over these properties can be of paramount importance for *in vivo* applications. However, in many cases fine-tuning of size, shape, and physicochemical properties of nanoparticles is difficult to achieve. Having a library of diverse size nanoparticles with tunable properties is advantageous, as pharmacokinetic mechanisms of drug delivery, distribution, and clearance are hard to predict.[40−43] These facts are the motivation behind the development of a simple method to tune the size and thermodynamic and chemical properties of RNA nanoparticles.

The complexity of RNA's tertiary structure complicates *de novo* design of such nanostructures; however, by utilizing a predefined 3D motif as the design template many complications can be avoided. This approach utilizes a modular design technique, sometimes referred to as RNA biomimetics. It involves the use of predefined structural motifs taken from biology as building blocks to construct RNA nanostructures of defined shape and size for a variety of applications including nanomedicine.[17,44] The use of predefined RNA motifs has been shown to be a successful method toward the rational design of RNA nanoarchitectures.[1,16,20,33] Naturally, the first step in applying the pRNA-3WJ in modular design was to construct triangles based on the native 60° angle of the pRNA-3WJ motif (Figure 1A),[23] ideal for the construction of an equilateral triangle. Utilizing this native angle, triangular nanoparticles were constructed using the modular design technique.[45] To create more diversity in size and shape, square-shaped geometry was the next goal. By stretching the 3WJ, a triangle, square, and pentagon can be formed.[46] The next question to be addressed is whether we can tune the size of one polygon by using the same 3WJ while altering the length of each side of the square.

In this report, we show the construction of multiple variants of square-shaped RNA architectures based on a modular design technique using the same core structure, the pRNA-3WJ. By simply increasing or decreasing the length of the RNA duplex between each corner of the square, nanoparticles of 5, 10, and 20 nm were constructed with diverse thermal stabilities. The thermodynamic stability of certain RNA tertiary motifs and the strong Watson−Crick base pairing in RNA folding and base stacking ensure predictability in structure that makes it possible to increase or decrease size by simply adding or removing nucleotides, directly affecting size. Further control over nanoparticle stability was demonstrated by modulating the oligonucleotide used as the "core" strand during construction of the square nanoparticle. Exploiting the different stabilities of RNA, DNA, and 2′-fluorine-modified (2′F) RNA, it is possible to add another dimension of regulation over the physicochemical properties of RNA nanoparticles. Moreover, due to the unique construction technique used, we show that it is possible to completely avoid intermolecular interactions such as kissing-loop and sticky-end interactions during construction of the nanoparticles. The potential of using the resulting RNA square assembly for biomedical and imaging applications is evidenced by the incorporation of therapeutic RNA, ribozyme, and fluorogenic aptamers. As shown here, the assembly properties and tunability of RNA nanoparticles can be easily exploited to determine a suitable combination of size and stability for a wide array of applications.

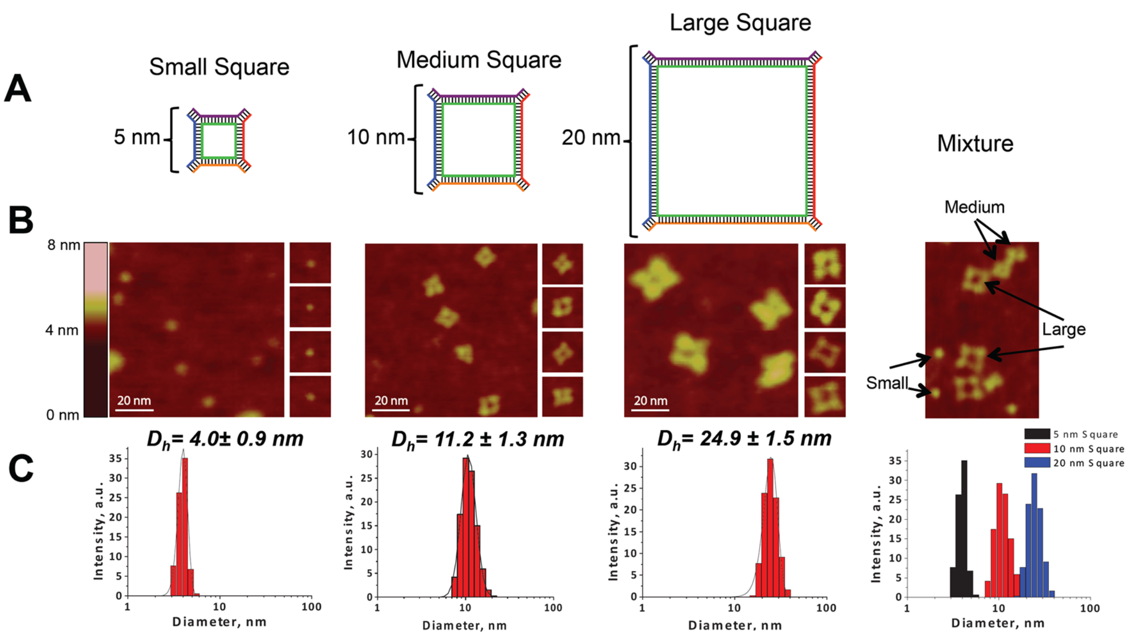

Figure 2. Physical properties of the RNA squares. (A) Schematic of small, medium, and large squares drawn to scale for size comparison. Four external strands (blue, purple, red, orange) are complementary to the core internal strand (green). (B) AFM imaging of small, medium, and large RNA squares. Zoomed pictures of individual squares located on the right. On the far right is a mixture of squares; each square is indicated by arrows. (C) Dynamic light scattering (DLS) to determine the size of square nanoparticles. Far right panel shows comparison of all three square constructs.

RESULTS AND DISCUSSION

RNA Square Design. Square-shaped RNA nanoarchitectures were designed *in silico* utilizing the planar geometry of the 3WJ structural motif. Swiss PDB Viewer (www.spdbv.vital-it.ch) was used to align four 3WJ building blocks (PDB ID: 4KZ2)[23] in a planar configuration utilizing the internal ~60° angle, created by helix one (H1) and helix two (H2), at each corner of the square (Figure 1A). A-type duplex RNA was then inserted to connect H1 and H2 (Figure 1A). The resulting design featured a square with four "arms" extending outward from each vertex of the square, facilitating the incorporation of additional RNA sequences, motifs, or functionalities. The final square contains five RNA strands, whereby four short strands (A, B, C, D) are complementary to one long "core" strand, E (Figure 1B, Supplemental Figure 1). This results in a nanoparticle containing a 3WJ at each vertex and A-type duplex RNA along each edge. Extension of both the core and external strands by increasing the number of complementary nucleotides was exploited to obtain RNA squares with variable but predictable sizes (Figure 2A). By such means, small, medium, and large square architecture were designed using Swiss PDB Viewer, and the sequences for all five strands were optimized to avoid nonspecific interactions using the Mfold program.[47]

Structural Characterization. Based on models, the sizes of the resulting square structures should be 5.1, 10.2, and 20.1 nm along each edge. The size increase results from extension of the duplex RNA connecting the 3WJs at each corner. On the basis of nearest neighbor thermodynamic parameters, larger size squares are expected to exhibit increased thermodynamic stability. As none of the 3WJ angles have a right angle according to its crystal structure (Figure 1A), the 3WJ motif must be stretched from ~60° to ~90° to accommodate square geometry. As a result, efficiency of self-assembly might be decreased. Consequently, our first experiments were aimed at characterizing the physical properties of the square constructs.

Native PAGE was first used to test the assembly and analyze assembly efficiency. Nanoparticle assembly was performed *via* a "one-pot" self-assembly procedure by thermal denaturation of all RNA strands in TMS buffer (40 mM Tris, 10 mM $MgCl_2$, 100 mM NaCl) and gradual cooling over 1 h. ImageJ software was used to analyze the intensity of gel bands and the yield of correctly folded 10 and 20 nm squares was estimated to be more than 90%, with a slight decrease in folding efficiency observed for the 5 nm square (Figure 1C). Additionally, the hypothesis that each strand was involved in the assembly, and that strand substitution was not occurring, was tested. For this assay, each strand A through E was fluorescently labeled. Five different squares, each with one of five strands labeled, were then assembled and analyzed by native PAGE. The results demonstrate that each strand contributes to the assembly and therefore the overall stability of the square (Supplemental Figure 3).

While native PAGE experiments suggest the formation of compact, homogeneous, and distinct RNA nanoparticles, atomic force microscopy (AFM) was performed to demonstrate the formation of the square-shaped RNA nanoarchitecture (Figure 2B). Resulting AFM images strongly support the formation of the medium and large square-shaped RNA architecture. Image resolution of RNA nanostructures is in many cases limited by tip size. Due to the resolution limits of the AFM images shown in this report, the small square appears only as dots with no square geometry obviously visible. The results are as expected, as the size of the small square model is 5.2 nm, a size too small to be clearly resolved. A small percentage of squares appear as diamond shaped, straying from square geometry. This can be attributed to the fact that AFM images were taken in air and not in solution, distorting the 3D shape when the nanoparticles are dried onto the mica surface. Alternatively, diamond shapes could be due to the slight flexibility of the 3WJ.[23] Using the large-square AFM images, particles were manually counted to determine the efficiency of assembly by AFM. It was revealed that the large square formed with 70% efficiency.

When considering a nanoparticle for use as an *in vivo* therapeutic, the size of the particle greatly affects the delivery efficacy. Too small a size and the particle will simply be excreted; too large a size and entry into the cell will be greatly hindered. Previous studies showed that the optimal size for the cellular uptake of nanoparticles is 10–50 nm.[1,48−51] Using dynamic light scattering (DLS), the average hydrodynamic diameters (D_h) of RNA square nanoparticles were determined to be 4.0 ± 0.9, 11.2 ± 1.3, and 24.9 ± 0.5 nm for the small, medium, and large size squares, respectively (Figure 2C). These values are in close agreement with the predicted size of the model structures. At sizes of 4.0, 11.2, and 24.9 nm we have constructed variable-size nanoparticles with potentially diverse physicochemical properties.

We have presented a simple method to adjust the size of RNA nanoparticles; however we aim to show that adjustment of size leads to diverse thermodynamic properties among square variants. To compare the thermodynamic stability of the squares, temperature gradient gel electrophoresis (TGGE) was used to determine the melting temperatures (T_M) of each square (T_M = 50% square formation). A temperature gradient perpendicular to electrical current was applied, and increasing T_M corresponding to an increase in size was observed (Supplemental Figure 2). Due to the fact that each of the square constructs contains four 3WJ motifs, the increase in melting temperature can be attributed directly to an increase in the amount of base-pairing in the structures. This trend follows the nearest neighbor predicitons for increasing of thermodynamic stability.

Taken together, structural analysis by computer modeling, DLS, and AFM suggest the formation of compact, flat, square RNA nanoparticles. The native geometry, determined by crystallization, has H1 and H2 of the 3WJ in a planar configuration.[23] The computer model also results in a planar geometry based on duplex alignment of connecting helices H1 and H2, strongly supporting the formation of planar square nanoparticles. Furthermore, the presence of square structures on AFM, and not triangular shapes, which would result from a 3D tetrahedron-like structure,[52] also supports a flat, square geometry. As expected, AFM imaging demonstrates the size differences among the small, medium, and large squares.

Previously, RNA triangles have been constructed using the same pRNA-3WJ.[45] After analysis of the square nanoparticle, it was determined that the square and triangle display diverse properties in thermodynamic stability, size, shape, and stoichiometry, functions possible per nanoparticle. Although not explored in depth in this study, it is possible that utilizing these particles in different applications, where size and shape play an important role, could be beneficial.

Physicochemical Properties Are Tunable. Native RNA structures are inherently sensitive to degradation by cellular nucleases, potentially limiting the application of RNA nanoparticles in clinical applications. Modifications to RNAs, such as 2′F modification on the ribose sugar of the RNA backbone, have been shown to reduce their sensitivity to cellular nucleases.[2,53] These same 2′F modifications have also been shown to increase the thermodynamic stability of RNA nanoparticles.[31] DNA has also proven to be more resistant to the degradation caused by cellular nucleases.[1] In order to be useful as an *in vivo* therapeutic, modifications must be made to the native square nanoparticles to gain resistance to RNase while retaining the same structure. Previous studies demonstrating different chemical and thermodynamic stabilities of the pRNA-3WJ constructed of RNA, DNA, and 2′F-RNA were the driving force behind the replacement of the core strand of the square nanoparticle.[31,53] Due to these diverse stabilities, it was predicted that replacement of the core strand with different oligoneucleotides would result in a nanoparticle with diverse physicochemical properties.

To impart tunable chemical and thermodynamic stabilities onto the 10 nm square nanoparticle, the internal core strand E was replaced with both 2′F-C/U-modified RNA and single-stranded DNA. Analysis by native PAGE demonstrated that all of the nanosquares co-migrated, indicating formation of the same geometry (Figure 3A). Moreover, all nanoparticles assembled with comparable yields of ~90% as determined by integration of the intensity of gel bands (Figure 3A).

A degradation assay in fetal bovine serum (FBS) was performed on each 10 nm hybrid square assembly. It was observed that substitution of the 2′F-modified core strand for unmodified RNA greatly enhances the stability of the nanoparticles in FBS (Figure 3B). After 14 h, ~92% of square nanoparticles with a 2′F-modified

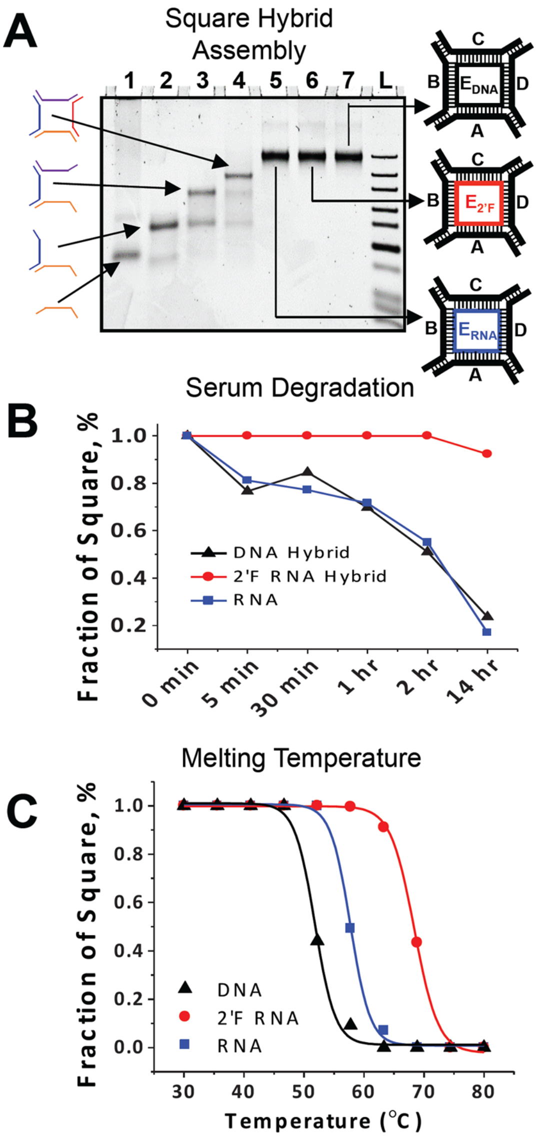

Figure 3. Comparison of RNA, 2′F-RNA, and DNA core strand hybrids. (A) Structure and native PAGE assembly of square nanoparticle hybrids. Blue strands represent RNA, red strands represent 2′F-RNA, and black strands represent DNA. Lanes 1 through 4 show the stepwise assembly from monomer to tetramer. (B) Nanoparticle stability in serum was compared among the square hybrid constructs. (C) TGGE melting temperature profiles of a square RNA nanoparticle along with 2′F and DNA core strand hybrids.

core strand remained, as compared to ∼20% for square nanoparticles with RNA and DNA core strands (Figure 3B, Supplemental Figure 4). While different hybrid duplexes exhibit different stabilities or susceptibilities to different RNases,[54,55] serum comparison mimics more closely an *in vivo* environment and allows direct comparison of each hybrid square. Overall, resistance to nuclease degradation was enhanced by replacing the core strand with 2′F-modified RNA.

To further examine the effect the core strand has on square nanoparticle stability, TGGE analysis was performed to determine the T_M of each hybrid. A temperature gradient, perpendicular to the electrical current, was applied from 40 to 80 °C. The T_M's for the 2′F-RNA, RNA, and DNA hybrid square nanoparticles were calculated to be 68.4, 57.7, and 51.8 °C, respectively (Figure 3C, Supplemental Figure 5). Melting temperatures were determined in 0.2 mM $MgCl_2$, simulating physiological conditions in which the cytoplasmic magnesium ion concentration is generally lower than 1 mM. At 10 mM magnesium concentrations no melting below 80 °C was observed (Supplemental Figure 5D, E, and F). Tertiary structure greatly affects the melting temperature, and therefore thermodynamic stability, of an RNA structure. The duplex cannot be solely responsible for the trend in melting temperature from the 2′F-RNA hybrid to the DNA-RNA hybrid since a large portion of each structure is 3WJ. It has been shown that complicated tertiary structures are more stable in RNA than DNA, resulting in a less stable DNA−RNA hybrid 3WJ.[31] Interestingly, the melting temperatures correlate with the FBS resistance assay, indicating that the 2′F-RNA hybrid square was the most stable, followed by the native RNA square, and the DNA hybrid architecture was the least stable.

In clinical applications, considering pharmacokinetics, biodistribution, and toxicity, the most stable nanoparticles will not always be the most effective treatment.[41−43] Our results show that it is possible to tune the stability characteristics of the RNA square nanoparticles by substituting the core strand and varying the ratio of 2′F nucleotides. This simple modification produces physicochemically diverse structures that can be easily tuned based on application.

Functionalizing the Square Scaffold. In order for the square architecture to be useful as a potential therapeutic in nanomedical applications, functional molecules (RNAi, aptamers, ribozymes) must be successfully fused into the core structure while it retains native folding and properties. Thus, the question of whether or not the RNA scaffold can harbor different RNA functional moieties such as siRNA, ribozymes, and RNA fluorogenic aptamers was addressed. More importantly, whether the functional molecules retain their activity when incorporated into the square scaffold was assessed.

As such, four functional RNA groups, RNA spinach (SPIN) aptamer,[56] RNA malachite green (MG) aptamer,[57,58] hepatitis B virus (HBV) ribozyme,[59] and siRNA targeting luciferase gene,[60] were incorporated at each corner of the 10 nm square nanoparticle (Figure 4A, Supplemental Figure 6). The multifunctional square assembly showed more than 90% efficiency, as analyzed by integration of gel bands (Figure 4B). Additional AFM imaging was performed to demonstrate the retention of square geometry with the fused functionalities (Figure 4C).

The MG and SPIN aptamers are synthetic RNA aptamer sequences, previously obtained through SELEX (Systematic Evolution of Ligands by Exponential Enrichment),[61] that bind the malachite green and

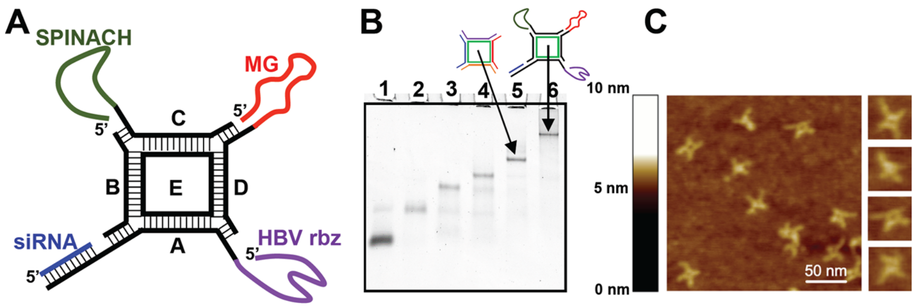

Figure 4. Design and assembly of a multifunctional square. (A) Illustration of square structure with spinach (SPIN) aptamer, malachite green (MG) aptamer, hepatitis B virus (HBV) ribozyme, and luciferase siRNA incorporated into the square. (B) Assembly of the square nanoparticle and multifunctional square assessed by 7% native PAGE. (C) AFM images of multifunctional square nanoparticles with functional moieties visible on the corners.

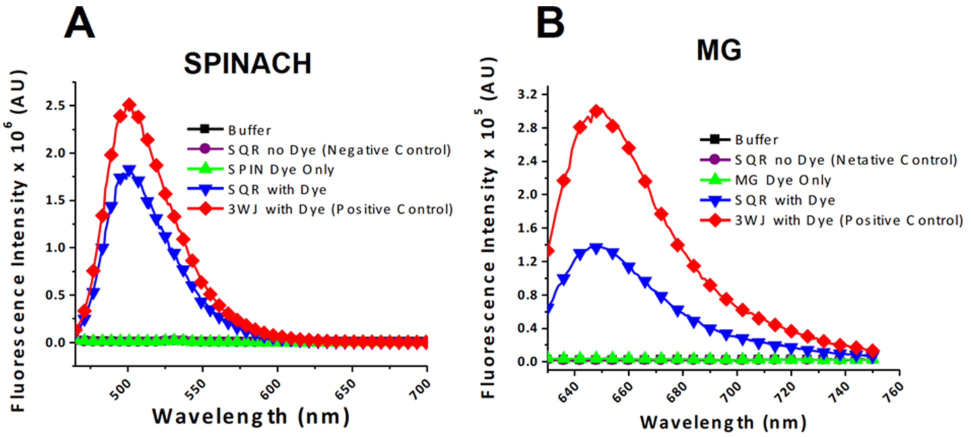

Figure 5. Fluorescence assays for a multifunctional square. (A) Spinach aptamer assay. Increased fluorescence is shown upon incubation with DFHBI dye. (B) Malachite green aptamer assay. Increased fluorescence is shown upon incubation with malachite green dye.

DFHBI dyes, respectively.[56,58,62,63] Free fluorophores in solution do not exhibit fluorescence and emit light only upon binding to their correctly folded RNA aptamer structures.[64,65] To assay if folding was retained when incorporated into the multifunctional square, fluorometer measurements were taken for the triphenylmethane and DFHBI chemicals alone and in the presence of the functional RNA square (Figure 5). The multifunctional square was simultaneously incubated with both fluorophores, and fluorescence measurements were then taken. Both aptamers retained their folding and bound their respective fluorophore as evidenced by an increase in triphenylmethane and DFHBI emission upon binding. As a positive control, a 3WJ with the MG aptamer and the SPIN aptamer were used, both of which have been previously shown to exhibit increased fluorescence signal when incubated with their respective fluorophores.[2,63] Furthermore, we aimed to show the simultaneous dual-mode fluorescent properties of the functional square architecture. The PAGE gel was stained for both MG and spinach aptamer dyes. Individual fluorescence of each aptamer was detected when incorporated into the same nanoparticle (Supplemental Figure 7).

The HBV ribozyme is a hammerhead ribozyme that cleaves hepatitis B genomic RNA. Ribozymes show potential as therapeutic agents; however they traditionally have shown low efficiency when tested *in vivo*. This can be attributed to the misfolding of ribozymes in an intracellular environment and their susceptibility to exonucleases.[66] One method to protect the ribozymes and prevent their misfolding is to harbor them in larger, more complex structures. However, ribozymes must maintain their native folding, to retain functionality, when fused to RNA or incorporated into nanoparticles. Upon incubation of the multifunctional square with HBV genomic RNA, cleaveage of the RNA genome occurs. Figure 6A demonstrates that the HBV ribozyme retains its catalytic activity when fused with the RNA square, as the cleaved products are clearly seen on the gel and the bands are comparable with a positive pRNA-HBV control construct.[66]

To test the ability of the RNA square to carry siRNA for gene-silencing effects, an *in vitro* assay was performed with a dual-luciferase reporter system.[62] An siRNA antisense strand, which targets the firefly luciferase gene, was hybridized with its complementary sense strand used as a sticky end fused onto the multifunctional square (Figure 4A). A decrease in target gene,

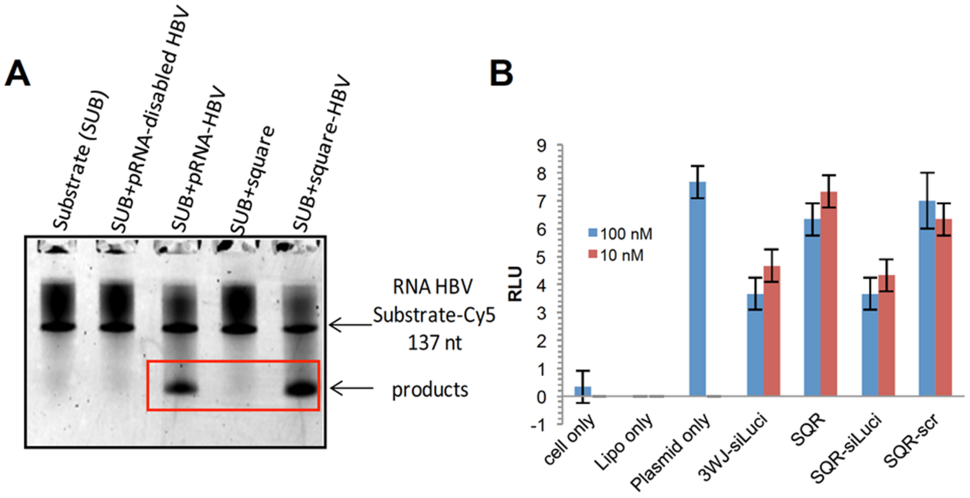

Figure 6. Ribozyme and siRNA activity assay. (A) Catalytic activity of the HBV ribozyme. Cleaved products are boxed. pRNA-HBV-Rbz was used as a control (B) Luciferase siRNA activity assay. Gene knockdown was measured by a decrease in luminescence. Cell only, Lipofectamine (Lipo) only, and plasmid only were used as controls. Plasmid only control will exhibit the highest luminescence, as the cells are transfected only with plasmid and no RNA. For a positive control 3WJ-siRNA showing knockdown was used. As negative control, a naked square (no luciferase siRNA) and a scrambled siRNA sequence fused onto a square were used. The square tested contained all four functional moieties. RLU is relative luminescence units.

firefly, luminescence compared to reference gene, renilla, luminescence, indicates a decrease in target gene protein production, designating a positive result. In comparison to the positive control, a 3WJ nanoparticle with fused luciferase siRNA,[62] the multifunctional square harboring luciferase siRNA caused a similar decrease in luminescence, indicating similar gene knockdown activity (Figure 6B). Overall, the results indicated that the RNA square nanoparticles carrying luciferase siRNA displayed ~40% gene knockdown activity.

In order for DICER to recognize and process double-stranded (ds) RNA, the 3′-overhang must be accessible and not trapped inside the inner cavity of the square nanoparticle. This possible obstruction proves to be no vproblem. This newly constructed square makes it simple to incorporate other diverse functional moieties into one of the four "arms" of the square. This can be done by simply fusing siRNA into one of the four external scaffold strands.

The results demonstrate that diverse functionalities retain their activity when incorporated into the square scaffold, making the RNA square an addressable and programmable polyfunctional nanoscaffold for potential delivery of RNA therapeutics for application in medicine. Due to the unique five-strand construction of the square architecture, functionalities such as RNA aptamers and siRNA for gene therapy can be added by simply encoding for functionalities in the primary sequence of one strand in the square.

CONCLUSION

Here we report the design and construction of polyfunctional RNA square architectures utilizing the 3WJ motif of bacteriophage phi29. The conserved 60° angle from the 3WJ was expanded to 90°, and formation of square geometry was achieved. The length of the connecting helix was increased or decreased to generate three distinct sizes of nanoparticles. These three sizes of nanoparticles demonstrate diverse thermodynamic stabilities. By modulating the oligonucleotide used as the core strand we were able to tune the physicochemical properties of the square scaffold. The four arms extending from the four corners of the square were used to incorporate RNA functionalities, each of which was demonstrated to fold independently and correctly while retaining their authentic functionalities. The square nanoscaffold shows great promise for biomedical and imaging applications due to its tunable thermodynamic and biochemical stabilities. The technique shown here for simple design to finely tune physicochemical properties adds a new angle to exploit RNA nanoparticles in a clinical setting.

MATERIALS AND METHODS

RNA Synthesis, Purification, and Labeling. RNA oligomers were prepared by *in vitro* T7 transcription from dsDNA containing the T7 promoter prepared by polymerase chain reaction (PCR). Single-stranded (ss) DNA oligomers were purchased from Integrated DNA Technologies.

Cy5 whole chain labeling was carried out on the RNA oligomers following the Mirus Cy5 Label IT Nucleic Acid whole chain labeling procedure.

For TGGE analysis of core strand hybrid squares, the PerkinElmer [γ-^{32}P]-ATP was used to label one of the short external strands at the 5′ end.

Assembly of RNA Nanoparticles. Equimolar amounts of RNA oligomers were mixed to a final concentration of 1 μM in TMS buffer (40 mM Tris-HCl, 10 mM $MgCl_2$, 100 mM NaCl). The mixture was heated to 80 °C for 5 min and then slowly cooled to 4 °C at a rate of 2 °C/min on an Eppendorf Mastercycle thermocycler. Confirmation of the assembly products were then run on native PAGE (described below).

Native PAGE and TGGE Analysis. All assembly experiments were performed on 7% (29:1) native PAGE and run at 100 V in a 4 °C cold room for 120 min. Cy5-labeled RNAs were then scanned on a Typhoon FLA 7000, and total RNAs were stained with ethidium bromide (EB).

TGGE analysis was performed on 7% native PAGE in a buffer containing 50 mM TRIS pH = 8.0, 100 mM NaCl, and 0.2 mM $MgCl_2$. A gradient temperature of 40−75 °C was applied perpendicular to the electrical current, and the experiment was run for 1 h at 20 W. A total RNA concentration of 80 nM was used in the TGGE analysis of the core strand hybrid constructs, and a 100 nM RNA concentration was used for TGGE comparison of the different sized squares.

Apparent T_M values corresponded to the temperature at which half of the square fractions were dissociated, and apparent T_M values for multiple RNA strands were calculated as described previously (Supplemental Figure 5).[20]

Quantification analysis was performed using ImageJ software.[67] Equal-sized boxes were drawn around the lanes corresponding to the square complexes, and corresponding quantified values for each hybrid square were divided by the sum of the values presented in the corresponding lane. All plots were generated using OriginPro 8 software.

AFM Imaging. AFM images were taken using a MultiMode AFM NanoScope IV system (Veeco), as per previously reported methods.[68] Briefly, the RNA samples were diluted with TMS buffer to a final concentration of 3−5 nM. Then, a droplet of samples (5−10 μL) was immediately deposited on the specifically modified APS mica surface,[69,70] excess samples were washed with DEPC-treated water and dried under a flow of argon gas. AFM images in air were acquired using a MultiMode AFM NanoScope IV system (Veeco/Digital Instruments, Santa Barbara, CA, USA) operating in tapping mode.

FBS Resistance Assay. The square nanoparticles with RNA, 2′F RNA, and DNA core strands were incubated in 2% FBS solution at 37 °C for 14 h. After removal from 37 °C incubation after their respective time points, the samples were frozen on dry ice to prevent any further degradation. The samples were then analyzed on 7% native PAGE. ImageJ software was used to integrate the intensities of the assembled square nanoparticles in the gel. Integration areas for each time point were compared to the integration area for the 0 min time point to construct an RNase degradation comparison between the RNA, DNA, and 2′F-RNA hybrids (Figure 4B). All plots were generated using OriginPro 8 software.

Spinach and Malachite Green Aptamer Fluorescence Measurements. Native 7% PAGE was used to detect the fluorescence emission of fluorogenic nanoparticles. The gel was stained simultaneously in a mixture of 5 μM MG and 5 μM DFHBI and scanned for the MG-apt fluorescence λ_{exc} centered at 635 nm and for spinach-APT fluorescence λ_{exc} centered at 473 nm. After recording images at different excitation wavelengths the total RNA stain in EB solution was performed to detect all RNAs in the gel.

Fluorescence emission in solution was measured, as previously reported.[63] Briefly, assembled square nanoparticles (0.1 μM) harboring MG and spinach aptamers in TMS buffer were mixed with MG (2 μM) and DFHBI (2 μM) (Lucerna, Inc., http://www.lucernatechnologies.com) and incubated at room temperature for 30 min (Figure 3e and f). Fluorescence was measured using a fluorospectrometer (Horiba Jobin Yvon), excited at 450 nm (565−750 nm scanning for emission) for spinach and 615 nm (625−750 nm scanning for emission) for MG dyes.

Dual Luciferase Assay. Experiments were carried out as previously described.[71] For square experiments carried out here, controls of cell only, plasmid only, and Lipofectamine 2000 (Lipo) only were used. Cell only contains luminescence data of cells only, with no transfection reagent or plasmid DNA. Lipo only samples contained just Lipofectamine 2000 transfection reagent. The plasmid-only samples contained DNA plasmid only, which were transfected into the cell utilizing the transfection reagent Lipo. For RNA controls, the 3WJ with luciferase siRNA was used, which has previously been shown to cause knockdown.[62] A square scaffold and a square utilizing scrambled siRNA sequence were utilized as negative controls.

HBV Ribozyme Activity Assay. The HBV ribozyme activity assay was carried out as previously detailed.[66] Briefly, the HBV RNA substrate was 5′-Cy5 labeled using the Mirus Cy5 labeling kit. The labeled substrate was incubated with a square nanoparticle conjugated with HBV ribozyme for 60 min at 37 °C in buffer containing 20 mM $MgCl_2$, 20 mM NaCl, and 50 mM Tris-HCl (pH 7.5). pRNA conjugated to the HBV ribozyme served as a positive control, and pRNA with a disabled HBV ribozyme was used as a negative control. The cleaved fragments were analyzed on the Typhoon fluorescent imaging system.

Conflict of Interest: The authors declare the following competing financial interest(s): P.G. is a co-founder of Kylin Therapeutics, Inc., RNA Nano, LLC., and Biomotor and Nucleic Acid Nanotechnology Development Corp., Ltd.

Acknowledgment. We thank Luda Shlyakhtenko for AFM imaging at the Nanoimaging Core Facility supported by the NIH SIG program and the UNMC Program of ENRI to Y.L. The work was supported by NIH grants U01-CA151648 and R01-EB003730. Funding to Peixuan Guo's Endowed Chair in Nanobiotechnology position is from the William Fairish Endowment Fund. The content is solely the responsibility of the authors and does not necessarily represent the official views of the NIH. We would like to acknowledge the core facilities of the Markey Cancer Center at the University of Kentukcy.

Supporting Information Available: RNA sequences for all squares, additional assembly experiments, gel images for FBS and melting temperature assays, and secondary structures of the three squares and multifunctional square. These materials are available free of charge *via* the Internet at http://pubs.acs.org.

REFERENCES AND NOTES

1. Guo, P. The Emerging Field of RNA Nanotechnology. *Nat. Nanotechnol.* **2010**, *5*, 833–842.
2. Shu, D.; Shu, Y.; Haque, F.; Abdelmawla, S.; Guo, P. Thermodynamically Stable RNA Three-Way Junction for Constructing Multifunctional Nanoparticles for Delivery of Therapeutics. *Nat. Nanotechnol.* **2011**, *6*, 658–667.
3. Gu, H.; Chao, J.; Xiao, S. J.; Seeman, N. C. Dynamic Patterning Programmed by DNA Tiles Captured on a DNA Origami Substrate. *Nat. Nanotechnol.* **2009**, *4*, 245–248.
4. Seeman, N. C. DNA in a Material World. *Nature* **2003**, *421*, 427–431.
5. Service, R. F. Nanotechnology. Biology Offers Nanotechs a Helping Hand. *Science* **2002**, *298*, 2322–2323.
6. Craighead, H. G. Nanoelectromechanical Systems. *Science* **2000**, *290*, 1532–1536.
7. Fennimore, A. M.; Yuzvinsky, T. D.; Han, W. Q.; Fuhrer, M. S.; Cumings, J.; Zettl, A. Rotational Actuators Based on Carbon Nanotubes. *Nature* **2003**, *424*, 408–410.
8. Haque, F.; Lunn, J.; Fang, H.; Smithrud, D.; Guo, P. Real-Time Sensing and Discrimination of Single Chemicals Using the Channel of Phi29 DNA Packaging Nanomotor. *ACS Nano* **2012**, *6*, 3251–3261.
9. Gerion, D.; Parak, W. J.; Williams, S. C.; Zanchet, D.; Micheel, C. M.; Alivisatos, A. P. Sorting Fluorescent Nanocrystals with DNA. *J. Am. Chem. Soc.* **2002**, *124*, 7070–7074.
10. Wendell, D.; Jing, P.; Geng, J.; Subramaniam, V.; Lee, T. J.; Montemagno, C.; Guo, P. Translocation of Double-Stranded DNA through Membrane-Adapted Phi29 Motor Protein Nanopores. *Nat. Nanotechnol.* **2009**, *4*, 765–772.
11. Abdelmawla, S.; Guo, S.; Zhang, L.; Pulukuri, S.; Patankar, P.; Conley, P.; Trebley, J.; Guo, P.; Li, Q. X. Pharmacological Characterization of Chemically Synthesized Monomeric pRNA Nanoparticles for Systemic Delivery. *Mol. Ther.* **2011**, *19*, 1312–1322.

12. Wang, S.; Haque, F.; Rychahou, P. G.; Evers, B. M.; Guo, P. Engineered Nanopore of Phi29 DNA-Packaging Motor for Real-Time Detection of Single Colon Cancer Specific Antibody in Serum. *ACS Nano* **2013**, *7*, 9814–9822.
13. Kukowska-Latallo, J. F.; Candido, K. A.; Cao, Z.; Nigavekar, S. S.; Majoros, I. J.; Thomas, T. P.; Balogh, L. P.; Khan, M. K.; Baker, J. R., Jr. Nanoparticle Targeting of Anticancer Drug Improves Therapeutic Response in Animal Model of Human Epithelial Cancer. *Cancer Res.* **2005**, *65*, 5317–5324.
14. Ishikawa, J.; Furuta, H.; Ikawa, Y. RNA Tectonics (TectoRNA) for RNA Nanostructure Design and Its Application in Synthetic Biology. *Wiley Interdiscip. Rev. RNA* **2013**, *4*, 651–664.
15. Hansma, H. G.; Oroudjev, E.; Baudrey, S.; Jaeger, L. TectoRNA and 'Kissing-Loop' RNA: Atomic Force Microscopy of Self-Assembling RNA Structures. *J. Microsc.* **2003**, *212*, 273–279.
16. Jaeger, L.; Westhof, E.; Leontis, N. B. TectoRNA: Modular Assembly Units for the Construction of RNA Nano-Objects. *Nucleic Acids Res.* **2001**, *29*, 455–463.
17. Jaeger, L.; Chworos, A. The Architectonics of Programmable RNA and DNA Nanostructures. *Curr. Opin Struct. Biol.* **2006**, *16*, 531–543.
18. Leontis, N. B.; Westhof, E. Analysis of RNA Motifs. *Curr. Opin. Struct. Biol.* **2003**, *13*, 300–308.
19. Petrov, A. I.; Zirbel, C. L.; Leontis, N. B. Automated Classification of RNA 3D Motifs and the RNA 3D Motif Atlas. *RNA* **2013**, *19*, 1327–1340.
20. Shu, Y.; Haque, F.; Shu, D.; Li, W.; Zhu, Z.; Kotb, M.; Lyubchenko, Y.; Guo, P. Fabrication of 14 Different RNA Nanoparticles for Specific Tumor Targeting without Accumulation in Normal Organs. *RNA* **2013**, *19*, 766–777.
21. Haque, F.; Shu, D.; Shu, Y.; Shlyakhtenko, L.; Rychahou, P.; Evers, M.; Guo, P. Ultrastable Synergistic Tetravalent RNA Nanoparticles for Targeting to Cancers. *Nano Today* **2012**, *7*, 245–257.
22. Reblova, K.; Strelcova, Z.; Kulhanek, P.; Besseova, I.; Mathews, D. H.; Van Nostrand, K.; Yildirim, I.; Turner, D. H.; Sponer, J. An RNA Molecular Switch: Intrinsic Flexibility of 23S rRNA Helices 40 and 68 5 ′-UAA/5 ′-GAN Internal Loops Studied by Molecular Dynamics Methods. *J. Chem. Theory Comput.* **2010**, *6*, 910–929.
23. Zhang, H.; Endrizzi, J. A.; Shu, Y.; Haque, F.; Sauter, C.; Shlyakhtenko, L. S.; Lyubchenko, Y.; Guo, P.; Chi, Y. I. Crystal Structure of 3WJ Core Revealing Divalent Ion-Promoted Thermostability and Assembly of the Phi29 Hexameric Motor pRNA. *RNA* **2013**, *19*, 1226–1237.
24. Bindewald, E.; Hayes, R.; Yingling, Y. G.; Kasprzak, W.; Shapiro, B. A. RNAJunction: A Database of RNA Junctions and Kissing Loops for Three-Dimensional Structural Analysis and Nanodesign. *Nucleic Acids Res.* **2008**, *36*, D392–D397.
25. Guo, P.; Zhang, C.; Chen, C.; Trottier, M.; Garver, K. Inter-RNA Interaction of Phage Phi29 pRNA to Form a Hexameric Complex for Viral DNA Transportation. *Mol. Cell* **1998**, *2*, 149–155.
26. Shu, Y.; Shu, D.; Haque, F.; Guo, P. Fabrication of pRNA Nanoparticles to Deliver Therapeutic RNAs and Bioactive Compounds into Tumor Cells. *Nat. Protoc.* **2013**, *8*, 1635–1659.
27. Guo, P.; Haque, F.; Hallahan, B.; Reif, R.; Li, H. Uniqueness, Advantages, Challenges, Solutions, and Perspectives in Therapeutics Applying RNA Nanotechnology. *Nucleic Acid Ther.* **2012**, *22*, 226–245.
28. Guo, P. RNA Nanotechnology: Engineering, Assembly and Applications in Detection, Gene Delivery and Therapy. *J. Nanosci. Nanotechnol.* **2005**, *5* (12), 1964–1982.
29. Shu, D.; Moll, W. D.; Deng, Z.; Mao, C.; Guo, P. Bottom-Up Assembly of RNA Arrays and Superstructures as Potential Parts in Nanotechnology. *Nano Lett.* **2004**, *4*, 1717–1723.
30. Shu, Y.; Cinier, M.; Shu, D.; Guo, P. Assembly of Multifunctional Phi29 pRNA Nanoparticles for Specific Delivery of siRNA and Other Therapeutics to Targeted Cells. *Methods* **2011**, *54*, 204–214.
31. Binzel, D. W.; Khisamutdinov, E. F.; Guo, P. Entropy-Driven One-Step Formation of Phi29 pRNA 3WJ from Three RNA Fragments. *Biochemistry* **2014**, *53*, 2221–2231.
32. Afonin, K. A.; Kireeva, M.; Grabow, W. W.; Kashlev, M.; Jaeger, L.; Shapiro, B. A. Co-Transcriptional Assembly of Chemically Modified RNA Nanoparticles Functionalized with siRNA. *Nano Lett.* **2012**, *12*, 5192–5195.
33. Grabow, W. W.; Zakrevsky, P.; Afonin, K. A.; Chworos, A.; Shapiro, B. A.; Jaeger, L. Self-Assembling RNA Nanorings Based on RNAI/II Inverse Kissing Complexes. *Nano Lett.* **2011**, *11*, 878–887.
34. Afonin, K. A.; Grabow, W. W.; Walker, F. M.; Bindewald, E.; Dobrovolskaia, M. A.; Shapiro, B. A.; Jaeger, L. Design and Self-Assembly of pRNA-Functionalized RNA Nanoparticles for Use in Automated Nanomedicine. *Nat. Protoc.* **2011**, *6*, 2022–2034.
35. Afonin, K. A.; Bindewald, E.; Yaghoubian, A. J.; Voss, N.; Jacovetty, E.; Shapiro, B. A.; Jaeger, L. *In Vitro* Assembly of Cubic RNA-Based Scaffolds Designed *in silico*. *Nat. Nanotechnol.* **2010**, *5*, 676–682.
36. Severcan, I.; Geary, C.; Chworos, A.; Voss, N.; Jacovetty, E.; Jaeger, L. A Polyhedron Made of tRNAs. *Nat. Chem.* **2010**, *2*, 772–779.
37. Severcan, I.; Geary, C.; V, E.; C, A.; Jaeger, L. Square-Shaped RNA Particles From Different RNA Folds. *Nano Lett.* **2009**, *9*, 1270–1277.
38. Jaeger, L. Defining the Syntax for Self-Assembling RNA Tertiary Architectures. *Nucleic Acids Symp. Ser. (Oxf)* **2009**, 83–84.
39. Nasalean, L.; Baudrey, S.; Leontis, N. B.; Jaeger, L. Controlling RNA Self-Assembly to Form Filaments. *Nucleic Acids Res.* **2006**, *34*, 1381–1392.
40. Feng, L.; Li, S. K.; Liu, H.; Liu, C. Y.; LaSance, K.; Haque, F.; Shu, D.; Guo, P. Ocular Delivery of pRNA Nanoparticles: Distribution and Clearance after Subconjunctival Injection. *Pharm. Res.* **2014**, *31*, 1046–1058.
41. Moghimi, S. M.; Hunter, A. C.; Andresen, T. L. Factors Controlling Nanoparticle Pharmacokinetics: An Integrated Analysis and Perspective. *Ann. Rev. Pharmacol. Toxicol.* **2012**, *52*, 481–503.
42. Merkel, T. J.; Chen, K.; Jones, S. W.; Pandya, A. A.; Tian, S. M.; Napier, M. E.; Zamboni, W. E.; DeSimone, J. M. The Effect of Particle Size on the Biodistribution of Low-Modulus Hydrogel PRINT Particles. *J. Controlled Release* **2012**, *162*, 37–44.
43. Igarashi, E. Factors Affecting Toxicity and Efficacy of Polymeric Nanomedicines. *Toxicol. Appl. Pharmacol.* **2008**, *229*, 121–134.
44. Zhang, S. Fabrication of Novel Biomaterials through Molecular Self-Assembly. *Nat. Biotechnol.* **2003**, *21*, 1171–1178.
45. Khisamutdinov, E. F.; Jasinski, D. L.; Guo, P. RNA as a Boiling-Resistant Anionic Polymer Material to Build Robust Structures with Defined Shape and Stoichiometry. *ACS Nano* **2014**, *8*, 4771–4781.
46. Khisamutdinov, E.; Li, H.; Jasinski, D.; Chen, J.; Fu, J.; Guo, P. Enhancing Immunomodulation on Innate Immunity by Shape Transition among RNA Triangle, Square, and Pentagon Nanovehicles. *Nucleic Acids Res.* **2014**In press.
47. Zuker, M. Mfold Web Server for Nucleic Acid Folding and Hybridization Prediction. *Nucleic Acids Res.* **2003**, *31*, 3406–3415.
48. Prabha, S.; Zhou, W. Z.; Panyam, J.; Labhasetwar, V. Size-Dependency of Nanoparticle-Mediated Gene Transfection: Studies with Fractionated Nanoparticles. *Int. J. Pharm.* **2002**, *244*, 105–115.
49. Huang, X. L.; Teng, X.; Chen, D.; Tang, F. Q.; He, J. Q. The Effect of the Shape of Mesoporous Silica Nanoparticles on Cellular Uptake and Cell Function. *Biomaterials* **2010**, *31*, 438–448.
50. Dash, B. C.; Rethore, G.; Monaghan, M.; Fitzgerald, K.; Gallagher, W.; Pandit, A. The Influence of Size and Charge of Chitosan/Polyglutamic Acid Hollow Spheres on Cellular Internalization, Viability and Blood Compatibility. *Biomaterials* **2010**, *31*, 8188–8197.
51. Gratton, S. E. A.; Ropp, P. A.; Pohlhaus, P. D.; Luft, J. C.; Madden, V. J.; Napier, M. E.; DeSimone, J. M. The Effect of Particle Design on Cellular Internalization Pathways. *Proc. Natl. Acad. Sci. U.S.A.* **2008**, *105*, 11613–11618.

52. Li, Z.; Wei, B.; Nangreave, J.; Lin, C. X.; Liu, Y.; Mi, Y. L.; Yan, H. A Replicable Tetrahedral Nanostructure Self-Assembled from a Single DNA Strand. *J. Am. Chem. Soc.* **2009**, *131*, 13093–13098.
53. Liu, J.; Guo, S.; Cinier, M.; Shlyakhtenko, L.; Shu, Y.; Chen, C.; Shen, G.; Guo, P. Fabrication of Stable and RNase-Resistant RNA Nanoparticles Active in Gearing the Nanomotors for Viral DNA Packaging. *ACS Nano* **2010**, *5*, 237–246.
54. Goedken, E. R.; Marqusee, S. Native-State Energetics of a Thermostabilized Variant of Ribonuclease HI. *J. Mol. Biol.* **2001**, *314*, 863–871.
55. Cuchillo, C. M.; Nogues, M. V.; Raines, R. T. Bovine Pancreatic Ribonuclease: Fifty Years of the First Enzymatic Reaction Mechanism. *Biochemistry* **2011**, *50*, 7835–7841.
56. Paige, J. S.; Wu, K. Y.; Jaffrey, S. R. RNA Mimics of Green Fluorescent Protein. *Science* **2011**, *333*, 642–646.
57. Babendure, J. R.; Adams, S. R.; Tsien, R. Y. Aptamers Switch on Fluorescence of Triphenylmethane Dyes. *J. Am. Chem. Soc.* **2003**, *125*, 14716–14717.
58. Baugh, C.; Grate, D.; Wilson, C. 2.8 A Crystal Structure of the Malachite Green Aptamer. *J. Mol. Biol.* **2000**, *301*, 117–128.
59. Zhu, L. F.; Yi, R. D.; Lu, C. D.; Wang, Y.; Qi, G. Ribozyme That Site-Specifically Cleaves the RNA Fragment Derived from Core Antigen Gene of Hepatitis B Virus *in vitro*. *Chin. J. Biochem. Biophys.* **1994**, *26*, 239–249.
60. Shu, Y.; Shu, D.; Diao, Z.; Shen, G.; Guo, P. Fabrication of Polyvalent Therapeutic RNA Nanoparticles for Specific Delivery of siRNA, Ribozyme and Drugs to Targeted Cells for Cancer Therapy. *IEEE/NIH Life Sci. Syst. Appl. Workshop* **2009**, 9–12.
61. Ellington, A. D.; Szostak, J. W. *In Vitro* Selection of RNA Molecules That Bind Specific Ligands. *Nature* **1990**, *346*, 818–822.
62. Reif, R.; Haque, F.; Guo, P. Fluorogenic RNA Nanoparticles for Monitoring RNA Folding and Degradation in Real Time in Living Cells. *Nucleic Acid Ther.* **2013**, *22* (6), 428–437.
63. Shu, D.; Zhang, L.; Khisamutdinov, E.; Guo, P. Programmable Folding of Fusion RNA Complex Driven by the 3WJ Motif of Phi29 Motor pRNA. *Nucleic Acids Res.* **2013**, *42*, e10.
64. Paige, J. S.; Nguyen-Duc, T.; Song, W.; Jaffrey, S. R. Fluorescence Imaging of Cellular Metabolites with RNA. *Science* **2012**, *335*, 1194.
65. Afonin, K. A.; Danilov, E. O.; Novikova, I. V.; Leontis, N. B. TokenRNA: A New Type of Sequence-Specific, Label-Free Fluorescent Biosensor for Folded RNA Molecules. *ChemBioChem* **2008**, *9*, 1902–1905.
66. Hoeprich, S.; ZHou, Q.; Guo, S.; Qi, G.; Wang, Y.; Guo, P. Bacterial Virus Phi29 pRNA as a Hammerhead Ribozyme Escort to Destroy Hepatitis B Virus. *Gene Ther.* **2003**, *10*, 1258–1267.
67. Collins, T. J. ImageJ for Microscopy. *Biotechniques* **2007**, *43*, 25–30.
68. Lyubchenko, Y. L.; Shlyakhtenko, L. S.; Ando, T. Imaging of Nucleic Acids with Atomic Force Microscopy. *Methods* **2011**, *54*, 274–283.
69. Lyubchenko, Y. L.; Shlyakhtenko, L. S. AFM for Analysis of Structure and Dynamics of DNA and Protein-DNA Complexes. *Methods* **2009**, *47*, 206–213.
70. Lyubchenko, Y. L.; Gall, A. A.; Shlyakhtenko, L. S.; Harrington, R. E.; Jacobs, B. L.; Oden, P. I.; Lindsay, S. M. Atomic Force Microscopy Imaging of Double Stranded DNA and RNA. *J. Biomol. Struct. Dyn.* **1992**, *10*, 589–606.
71. Guo, P.; Shu, Y.; Binzel, D.; Cinier, M. Synthesis, Conjugation, and Labeling of Multifunctional pRNA Nanoparticles for Specific Delivery of siRNA, Drugs and Other Therapeutics to Target Cells. *Methods Mol. Biol.* **2012**, *928*, 197–219.